Perfect transverse spin splitting by a single particle with bianisotropy

Wenjia Li,[1] Jinhui Shi,[1] Chunying Guan,[1,*] Zheng Zhu,[1] Yang Gao,[2] Shutian Liu,[3] and Jianlong Liu[1,†]

[1]*Key Laboratory of In-Fiber Integrated Optics of Ministry of Education, College of Physics and Optoelectronic Engineering, Harbin Engineering University, Harbin 150001, China*

[2]*College of Electronic Engineering, Heilongjiang University, Harbin 150080, China*

[3]*School of Physics, Harbin Institute of Technology, Harbin 150001, China*

(Received 27 May 2021; revised 28 November 2021; accepted 6 December 2021; published 14 December 2021)

Transverse spin splitting is a novel optical phenomenon which stems from the spin-orbit interaction of light. In this paper, we reveal the perfect transverse spin splitting in the scattered far-field of a single particle with bianisotropy. It is the result of the polarization twist effect caused by the omega-type bianisotropy of the structure in which the magnetic and electric fields interact in an unusual way and form a transverse spin dipole moment. Based on the dipole model, we conducted a detailed theoretical analysis of the relationship between the magnetoelectric coupling and the polarization state of the scattered far field. Our method reveals a physical mechanism of splitting the spin state of incident light which is regarded as a kind of giant spin Hall effect. Moreover, this perfect transverse spin splitting can also be understood by the separation of far-field polarization singularities. Our results provide a new platform for manipulating the spin state in the scattered far field and open an avenue for designing the spin structure.

DOI: 10.1103/PhysRevB.104.235418

I. INTRODUCTION

Transverse spin splitting in a scattered far field is a novel optical phenomenon [1,2] verified by the spin state separation in far-field scattering. It has attracted increasing attention on account of its great potential in antennas [3], optical metrology [4,5], optical sensing [6–8], and spin photonics devices [9]. Transverse spin splitting essentially belongs to the spin Hall effect of light that originates from the spin-orbit interaction of light [10,11]. It is a manifestation of the interaction between the spin angular momentum and the external orbital angular momentum of light, which is reflected in the transformation of the polarization state and propagation direction [12–15]. During the past decade, there has been considerable attention to the perfect transverse spin splitting [1,5,16,17]. The perfect transverse spin splitting means lateral splitting of polarized light with opposite chirality. For single particles, the previous methods usually rely on focused beams [1,5,16] and surface waves [17]. The basis for achieving perfect transverse spin splitting is to generate the transverse spin electric dipole moment of the particle. Whereas, it is a challenge to achieve the perfect transverse spin splitting based on the characteristics of a single particle without special light sources, and its physical nature remains to be explored.

Magnetoelectric coupling of particles corresponds to the mutual induction between electric and magnetic dipoles [18]. Particles with bianisotropy possess the characteristics of magnetoelectric coupling [19–22], which provides an additional degree of freedom in manipulating the light field and makes the mode interference more diverse. The bianisotropy of the particle could enhance the spin-orbit interaction of light, which is promising for intriguing optical phenomena. Optical fields could be effectively modulated by using bianisotropic metasurfaces which have been demonstrated in many key field transformations [23–26]. The metasurface is a composite of the antenna array, so it is different from a single particle in the mechanism and application. Recently, there have been growing interests in polarization-dependent optical manipulation by a single bianisotropic particle [27,28]. However, using an omega-type bianisotropic particle to achieve the transverse spin splitting has not been reported. The unusual property of the bianisotropic particle is a potential pathway to manipulate the polarization state in scattered far field, but the difficulty lies in how to effectively tailor the magnetoelectric coupling in an individual particle.

Polarization singularities are correlated with the spin state of light. There have been growing interests in polarization singularities by photonic structures [29–33]. The *C* point and the *L* point are two general types of polarization singularities that correspond to pure circular and linear polarizations, respectively. Similar to the periodic photonic structures, the scattered far field of a single particle also has polarization singularities but in real space [34–36]. Specifically, polarization singularity is a key factor in understanding the nature of the perfect transverse spin splitting.

In this paper, an omega-type bianisotropic particle is investigated to realize the perfect transverse spin splitting in the scattered far field. We give detailed analytical expressions to describe the relationship between the magnetoelectric coupling and the polarization state of the scattered far field. It is demonstrated that there are two routes to achieve the perfect transverse spin splitting. One is to construct a transverse spin electric dipole moment that can be realized by

*cyguan@163.com
†liujl@hrbeu.edu.cn

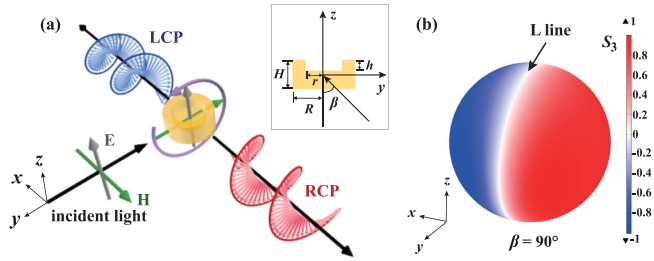

FIG. 1. (a) Schematic of perfect transverse spin splitting in the scattered far field of a bianisotropic particle. The inset shows the geometric view of the bianisotropic particle. (b) Normalized Stokes polarization parameter S_3 distribution of the perfect transverse spin splitting by a bianisotropic particle.

magnetoelectric coupling. The other is to utilize the transverse spin magnetic dipole moment that is achieved by electromagnetic coupling. In addition, the perfect transverse spin splitting is accompanied by the separation of polarization singularities. The methods and the results might provide practical guidelines for the further development of light manipulation, polarization sorters, and optical sensing.

II. THEORETICAL MODEL

The geometry model we considered is shown in Fig. 1(a) in which linearly polarized light incidents on a bianisotropic particle. The bianisotropic particle consists of a ceramic disk and a hollow with heights (H, h) and diameters (R, r). The incident direction of light is on the y-z plane, and the incident angle is β with respect to the z axis. We investigate the polarization state of the scattered far field of the bianisotropic particle. The red and blue rotatory arrows denote the right circular polarization (RCP) state and left circular polarization (LCP) state, respectively. Figure 1(b) depicts the normalized Stokes polarization parameter S_3 distribution of the perfect transverse spin splitting in scattered far field of a bianisotropic particle. S_3 is equal to 1 and -1, corresponding to RCP and LCP. The perfect transverse spin splitting means that the polarization states of opposite chirality are located on the left and right hemispheres, respectively. The linear polarization line (L line) is located on the middle boundary of the opposite hemisphere.

In the following analysis, CGS units are employed. The incident light field can be expressed as

$$\mathbf{E}_{\text{inc}} = E_0[A\hat{\mathbf{x}} + B(\cos\beta\hat{\mathbf{y}} + \sin\beta\hat{\mathbf{z}})]e^{ik_0(-\sin\beta y + \cos\beta z)}, \quad (1)$$

$$\mathbf{H}_{\text{inc}} = H_0[-B\hat{\mathbf{x}} + A(\cos\beta\hat{\mathbf{y}} + \sin\beta\hat{\mathbf{z}})]e^{ik_0(-\sin\beta y + \cos\beta z)}, \quad (2)$$

where $|A|^2 + |B|^2 = 1$, A and B could be real or imaginary that determine the polarization state of the incident electromagnetic field, k_0 is the wave number in a vacuum, and $E_0 = H_0 = 1$ are the amplitudes of the electric and magnetic fields. According to the dipole model, the electric field of the scattered far field can be written as

$$\mathbf{E} = \frac{k_0^2 e^{ik_0 r}}{r}[(\hat{\mathbf{n}} \times \mathbf{p}) \times \hat{\mathbf{n}} - \hat{\mathbf{n}} \times \mathbf{m}], \quad (3)$$

where $\hat{\mathbf{n}}$ is the unit direction vector, r is the distance from the center of the particle, and $\mathbf{p}$ and $\mathbf{m}$ are electric and magnetic dipole moments, respectively.

To realize a perfect transverse spin splitting by a single particle, we need a transverse spin electric dipole moment $\mathbf{p} = (p_x, p_y, p_z)^T = (0, \pm i, 1)^T$ or a transverse spin magnetic dipole moment $\mathbf{m} = (m_x, m_y, m_z)^T = (0, \pm i, 1)^T$. The superscript T denotes the transpose of a matrix. Here, we focus on the electric dipole model, whereas the magnetic model could be similar and will be discussed in Sec. IV. In general, the transverse dipole moment (e.g., p_z) can be excited directly because the incident light is always a transverse wave. For the longitudinal dipole moment (e.g., p_y), we can use the strategy of magnetoelectric coupling of the bianisotropic particle. For simplicity, we only consider the electric and magnetic dipole moments of the particle, neglecting quadrupoles and higher-order moments. The induced electric and magnetic dipole moments can be given by

$$\mathbf{p} = \overline{\alpha}_{\text{ee}} \cdot \mathbf{E}_{\text{inc}} + \overline{\alpha}_{\text{em}} \cdot \mathbf{H}_{\text{inc}}, \quad (4)$$

$$\mathbf{m} = \overline{\alpha}_{\text{me}} \cdot \mathbf{E}_{\text{inc}} + \overline{\alpha}_{\text{mm}} \cdot \mathbf{H}_{\text{inc}}, \quad (5)$$

where $\overline{\alpha}_{\text{ee}}$, $\overline{\alpha}_{\text{em}}$, $\overline{\alpha}_{\text{me}}$, and $\overline{\alpha}_{\text{mm}}$ are polarizability tensors. We consider the particle with omega-type bianisotropy [20]. The polarizability tensors of the particle read as [27]

$$\overline{\alpha}_{\text{ee}} = \begin{pmatrix} \alpha_{\text{ee}}^{xx} & 0 & 0 \\ 0 & \alpha_{\text{ee}}^{xx} & 0 \\ 0 & 0 & \alpha_{\text{ee}}^{zz} \end{pmatrix}, \quad (6)$$

$$\overline{\alpha}_{\text{mm}} = \begin{pmatrix} \alpha_{\text{mm}}^{xx} & 0 & 0 \\ 0 & \alpha_{\text{mm}}^{xx} & 0 \\ 0 & 0 & \alpha_{\text{mm}}^{zz} \end{pmatrix}, \quad (7)$$

$$\overline{\alpha}_{\text{em}} = \overline{\alpha}_{\text{me}} = \begin{pmatrix} 0 & i\gamma & 0 \\ -i\gamma & 0 & 0 \\ 0 & 0 & 0 \end{pmatrix}. \quad (8)$$

The magnetoelectric coupling strength is embodied in the value of γ in $\overline{\alpha}_{\text{em}}$ and $\overline{\alpha}_{\text{me}}$.

According to Eqs. (4) and (5), the electric and magnetic dipole moments $\mathbf{p}$ and $\mathbf{m}$ could be regulated by the incident light field. Assuming the incident light is linearly polarized along the z direction as shown in Fig. 1(a), the electric and magnetic components of the incident light could be written as $\mathbf{E}_{\text{inc}} = (0, 0, 1)^T$ and $\mathbf{H}_{\text{inc}} = (-1, 0, 0)^T$, respectively. According to Eqs. (4)–(8), the electric and magnetic dipole moments can be simplified as $\mathbf{p} = (p_x, p_y, p_z)^T = (0, i\gamma, \alpha_{\text{ee}}^{zz})^T$ and $\mathbf{m} = (m_x, m_y, m_z)^T = (\alpha_{\text{mm}}^{xx}, 0, 0)^T$, respectively. So far, we can get an ideal transverse spin dipole moment only if $m_x = 0$, the magnetoelectric coupling coefficient γ and the electric polarizability α_{ee}^{zz} are in-phase and have the same amplitude.

We plot the polarization distributions for the stand-alone electric dipoles p_y, p_z, and an ideal transverse spin moment $\mathbf{p} = (0, i, 1)^T$ in Figs. 2(a)–2(d), respectively. The color represents the Stokes polarization parameter S_3 and the arrows denote the directions of polarization. As shown in Fig. 2(d), the only L line is located on the boundary between the left and the right hemispheres, separating the left- and right-handedness fields. To show the polarization distribution more

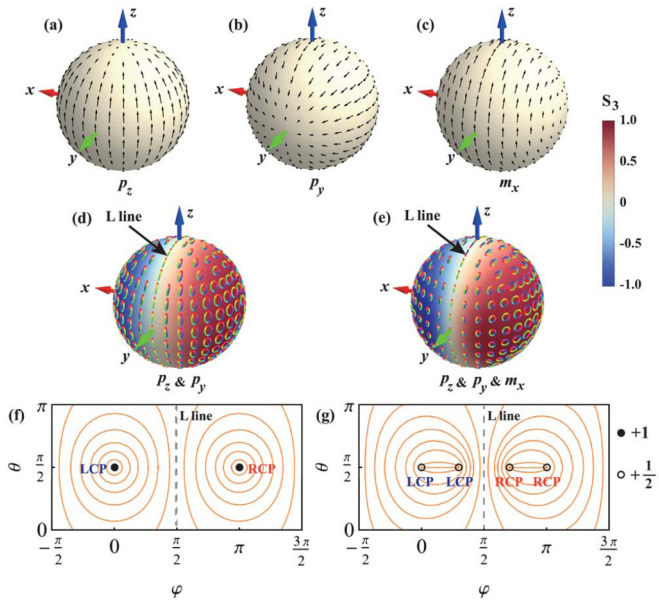

FIG. 2. Normalized Stokes polarization parameter S_3 and polarization distributions of an electric dipole (a) p_z, (b) p_y, (c) a magnetic dipole m_x, (d) an ideal transverse spin electric dipole moment $(p_y, p_z) = (i, 1)$, and (e) combination of the transverse spin electric dipole moment $(p_y, p_z) = (i, 1)$ and a magnetic dipole $m_x = -0.5$. (f) and (g) Projected polarization major axis for (d) and (e), respectively.

clearly, we project the major axis of the polarization ellipse in coordinates (θ, φ) and depict it in Fig. 2(f) [36–38]. Here, θ and φ denote the elevation angle and the azimuthal angle, respectively. The elevation angle (θ) is the angle with respect to the z axis, and the azimuthal angle (φ) represents the angle formed with respect to the x axis on the x-y plane. Two circularly polarized fields (C points) are located on the centers of the right and left hemispheres. The existence and evolution of C points are governed by the conservation of topological charge that is defined by the winding number of the polarization major axis around the point [36]. In Fig. 2(f), although these two C points have opposite handedness, they possess the identical topological charge $+1$.

Now, we move to investigate the influence of the magnetic dipole moment m_x. The normalized Stokes polarization parameter S_3 and the polarization distributions of a standalone magnetic dipole m_x are shown in Fig. 2(c). Comparing Figs. 2(a)–2(c), we can see that the polarization directions of the far field on the $x = 0$ plane are identical for these three dipoles. Superposing all these dipole moments ($p_y = i$, $p_z = 1$, $m_x = -0.5$), its far field [in Fig. 2(e)] is quite similar to that of the ideal transverse spin dipole [Fig. 2(f)]. The L line has not changed its position on the sphere. We also project the major axis of the polarization ellipses in coordinates (θ, φ) and depict it in Fig. 2(g). We can see that when m_x changes to -0.5, the winding pattern is stretched, and a pair of C points with identical topological charge $(+1/2)$ and handedness appear. The sign of m_x merely affects the emerging orientation of the new C point. The total topological charge $(+2)$ is conserved during the generation of the new C points. So, introducing the magnetic moment m_x with a certain

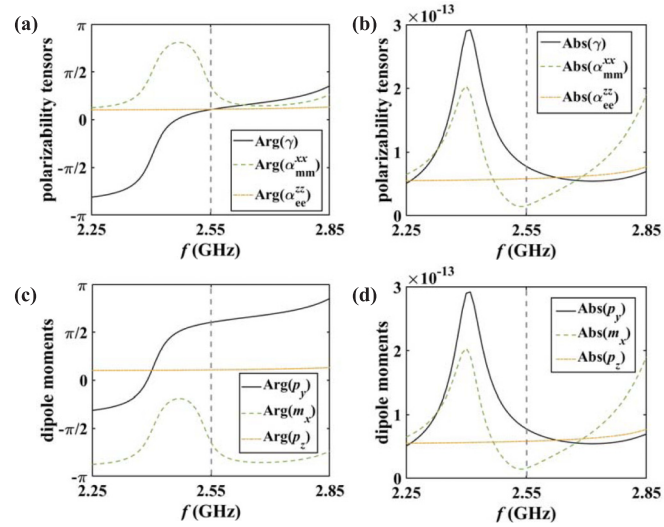

FIG. 3. Dependence in the (a) phase and (b) amplitude of the different components of the polarizability tensors with frequency. Dependence of the (c) phase and (d) amplitude of the different dipole moments on frequency.

amplitude compared with the electric moment will disturb the polarization distribution, but the spin state of the scattered far field is still perfectly split.

For a real particle with omega-type bianisotropy, we calculated its polarizability components and the induced electric and magnetic moments by simulation. Figures 3(a) and 3(b) show the change in the phase and amplitude of γ, $\alpha^{xx}_{\rm mm}$ and $\alpha^{zz}_{\rm ee}$ with the frequency f from 2.25 to 2.85 GHz. The diameter and height of the ceramic disk are $R = 15$ and $H = 12$ mm. The diameter and height of the hollow are $r = 9.4$ and $h = 4.5$ mm. It is clear that the curve of the polarizability $\alpha^{zz}_{\rm ee}$ is almost flat, but the magnetoelectric coupling coefficient γ exhibits a strong dispersion. The two curves in Fig. 3(a) cross with each other at about $f = 2.55$ GHz, which means that these two components are in phase. Moreover, their amplitudes are also close to each other at $f = 2.55$ GHz. The dependences of the phase and amplitude of the corresponding dipole moments (p_y, p_z, and m_x) on frequency f are presented in Figs. 3(c) and 3(d). The phase difference between p_y and p_z is almost 90° at $f = 2.55$ GHz and the amplitudes of p_y and p_z are close. The amplitude of m_x is quite smaller than that of p_y and p_z at $f = 2.55$ GHz. Therefore, we believe the perfect transverse spin splitting could be achieved at $f = 2.55$ GHz.

III. STOKES POLARIZATION PARAMETER S_3

We now derive the full expression of the scattered far field based on Eqs. (1)–(8) and investigate its polarization characteristics. In the spherical coordinate system, the scattered electric field can be divided into three components by r, elevation angle (θ), and azimuthal angle (φ). For the case of $A = 0$ and $B = 1$, θ and φ components of the scattered electric field can be obtained as

$$\mathbf{E}_\theta = \frac{k_0^2 e^{ik_0 r}}{r}\big[\sin\varphi\big(\alpha^{xx}_{\rm mm} - i\gamma\cos\beta + i\gamma\cos\theta + \alpha^{xx}_{\rm ee}\cos\beta\cos\theta\big) - \alpha^{zz}_{\rm ee}\sin\beta\sin\theta\big], \quad (9)$$

$$\mathbf{E}_\varphi = \frac{k_0^2 e^{ik_0 r}}{r}\cos\varphi\big(i\gamma - i\gamma\cos\beta\cos\theta + \alpha_{\mathrm{ee}}^{xx}\cos\beta + \alpha_{\mathrm{mm}}^{xx}\cos\theta\big). \tag{10}$$

In this paper, we investigate the polarization state of the scattered far field by the Stokes polarization parameters. At every point of the far field, the Stokes polarization parameter S_3 can be expressed as

$$\begin{aligned} S_3 &= -2\,\mathrm{Im}(E_\theta E_\phi^*) \\ &\propto -\cos\varphi\,\mathrm{Im}\{[\sin\varphi(\alpha_{\mathrm{mm}}^{xx} - i\gamma\cos\beta + i\gamma\cos\theta \\ &\quad + \alpha_{\mathrm{ee}}^{xx}\cos\beta\cos\theta) - \alpha_{\mathrm{ee}}^{zz}\sin\beta\sin\theta](-i\gamma^* \\ &\quad + i\gamma^*\cos\beta\cos\theta \\ &\quad + \alpha_{\mathrm{ee}}^{xx*}\cos\beta + \alpha_{\mathrm{mm}}^{xx*}\cos\theta)\}. \end{aligned} \tag{11}$$

Examining the factor $\cos\varphi$ in Eq. (11), it can be deduced that the ellipticity of the scattered far field is antisymmetric with respect to the y-z plane. Such antisymmetric polarization distribution in the opposite lateral hemisphere is referred to as the spin Hall effect of light. The Stokes polarization parameter S_3 falls to zero when $\varphi = 90^\circ$ that corresponds to the linearly polarized light. To describe the effect of polarization separation, we calculate the average normalized Stokes polarization parameter $\overline{S_3}$ in the opposite hemisphere for a monochromatic electromagnetic beam as

$$\overline{S_3^R} = \frac{\int_{-\pi/2}^{\pi/2}\int_0^{\pi} S_3 r^2\sin\theta\,d\theta\,d\varphi}{\int_{-\pi/2}^{\pi/2}\int_0^{\pi} S_0 r^2\sin\theta\,d\theta\,d\varphi}, \tag{12}$$

$$\overline{S_3^L} = \frac{\int_{\pi/2}^{3\pi/2}\int_0^{\pi} S_3 r^2\sin\theta\,d\theta\,d\varphi}{\int_{\pi/2}^{3\pi/2}\int_0^{\pi} S_0 r^2\sin\theta\,d\theta\,d\varphi}. \tag{13}$$

where $S_0 = |E_\theta|^2 + |E_\varphi|^2$ is the total intensity of the scattered far field, and $\overline{S_3^R}$ and $\overline{S_3^L}$ are the average normalized Stokes polarization parameters $\overline{S_3}$ in the right ($x > 0$) and left ($x < 0$) hemispheres separated by the y-z plane. By inserting Eqs. (9)–(11) into Eqs. (12) and (13), we obtain

$$\overline{S_3^R} = -2\pi\sin\beta\frac{\mathrm{Re}\big(\gamma^*\alpha_{\mathrm{ee}}^{zz}\big) - \cos\beta\,\mathrm{Im}\big(\alpha_{\mathrm{ee}}^{xx*}\alpha_{\mathrm{ee}}^{zz}\big)}{C_1 + C_2}, \tag{14}$$

$$\overline{S_3^L} = 2\pi\sin\beta\frac{\mathrm{Re}\big(\gamma^*\alpha_{\mathrm{ee}}^{zz}\big) - \cos\beta\,\mathrm{Im}\big(\alpha_{\mathrm{ee}}^{xx*}\alpha_{\mathrm{ee}}^{zz}\big)}{C_1 + C_2}, \tag{15}$$

$$C_1 = \mathrm{Re}\left[\frac{4}{3}i\pi\cos\beta\big(\gamma\alpha_{\mathrm{ee}}^{xx*} - \gamma^*\alpha_{\mathrm{ee}}^{xx} + \gamma^*\alpha_{\mathrm{mm}}^{xx} - \gamma\alpha_{\mathrm{mm}}^{xx*}\big) + \pi\left(2 + \frac{2}{3}\cos 2\beta\right)\gamma^*\gamma\right], \tag{16}$$

$$C_2 = \mathrm{Re}\left[\frac{2}{3}\pi(1+\cos 2\beta)\alpha_{\mathrm{ee}}^{xx*}\alpha_{\mathrm{ee}}^{xx} + \frac{2}{3}\pi(1-\cos 2\beta)\alpha_{\mathrm{ee}}^{zz*}\alpha_{\mathrm{ee}}^{zz} + \frac{4}{3}\pi\alpha_{\mathrm{mm}}^{xx*}\alpha_{\mathrm{mm}}^{xx}\right]. \tag{17}$$

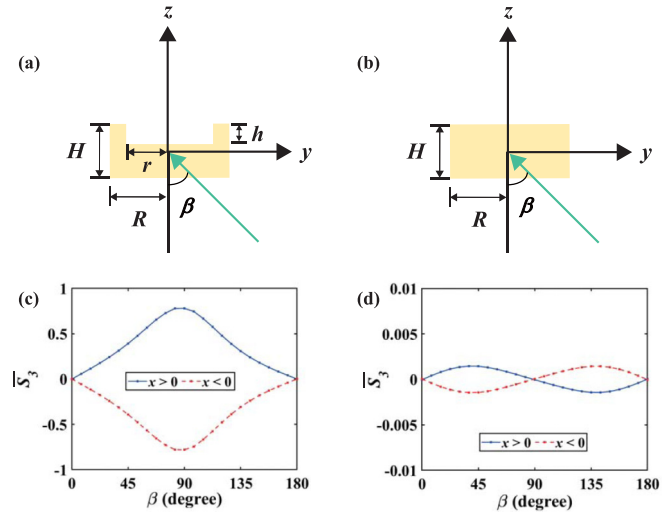

FIG. 4. (a) Geometric view of the bianisotropic particle consisting of a ceramic disk and a hollow. (b) Geometric view of the ceramic disk. (c) Dependence of $\overline{S_3}$ in the scattered far field on the incident angle for the bianisotropic particle. (d) Dependence of $\overline{S_3}$ in the scattered far field on the incident angle for the ceramic disk.

It indicates that the average normalized Stokes polarization parameters in the right and left hemispheres are opposite and are closely relevant to the polarizability tensors of the particle and the incident angle. The difference between $\overline{S_3^R}$ and $\overline{S_3^L}$ could present the spin Hall effect of light and evaluate the transverse spin splitting in the scattered far field. The perfect transverse spin splitting means the average Stokes parameter $\overline{S_3}$ in the opposite hemisphere is close to -1 and 1. As shown in Eqs. (14) and (15), the average Stokes parameter $\overline{S_3}$ in the opposite hemispheres ($x > 0$, $x < 0$) falls to zero at $\beta = 0^\circ$ (incidence along the positive z direction). The bianisotropy coefficient γ plays a decisive role in the spin splitting at $\beta = 90^\circ$ (incidence along the negative y direction).

IV. RESULTS AND DISCUSSIONS

To confirm the theoretical analysis, we give concrete examples by simulations with the finite element method (COMSOL MULTIPHYSICS). First, we investigate the difference of the polarization state in the scattered far field between the bianisotropic particle and the ceramic disk in the case of $A = 0$ and $B = 1$. The frequency of the incident linearly polarized light is 2.55 GHz. The geometric view of the bianisotropic particle consisting of a ceramic disk and a hollow is shown in Fig. 4(a). The diameter and height of the ceramic disk are R (= 15 mm) and H (= 12 mm). The diameter and height of the hollow are r (= 9.4 mm) and h (= 4.5 mm). The relative permittivity of ceramic is 39. Figure 4(b) shows the geometric view of the ceramic disk with diameter R and height H. Dependences of $\overline{S_3}$ in the scattered far field on the incident angle for the bianisotropic particle and the ceramic disk are illustrated in Figs. 4(c) and 4(d). The red and blue curves correspond to the left ($x < 0$) and right ($x > 0$) hemispheres, respectively. It proves that $\overline{S_3}$ of the left and right hemispheres are opposite. The left and right hemispheres have opposite polarization states. It is worth noting that $\overline{S_3}$ of

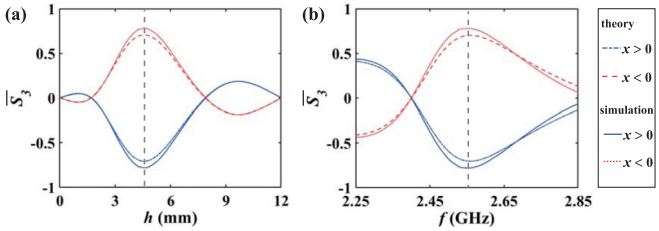

FIG. 5. (a) Dependence of $\overline{S_3}$ on the height h. (b) Dependence of $\overline{S_3}$ on the frequency f.

the bianisotropic particle is more than two orders of magnitude larger than that of the ceramic disk, which means the bianisotropy plays a key role in the transverse spin splitting. Considering this factor, $\overline{S_3}$ of the bianisotropic particle should change with the incident angle approximately according to the law of the sine function by Eqs. (14) and (15). $\overline{S_3}$ reaches its maximum value at $\beta = 90^\circ$ and is 0 at $\beta = 0^\circ$ and 180° for the bianisotropic particle as shown in Fig. 4(c). For the ceramic disk without bianisotropy, Eqs. (14) and (15) can be simplified as $\overline{S_3^R} = \pi \sin 2\beta \mathrm{Im}(\alpha_{ee}^{xx*}\alpha_{ee}^{zz})/C_2$ and $\overline{S_3^L} = -\pi \sin 2\beta \mathrm{Im}(\alpha_{ee}^{xx*}\alpha_{ee}^{zz})/C_2$ where $\overline{S_3}$ approximately varies as the sine function of twice the incident angle. $\overline{S_3}$ is 0 at $\beta = 0^\circ, 90^\circ$, and 180° for the ceramic disk as shown in Fig. 4(d). The dependent rules of $\overline{S_3}$ with β in Figs. 4(c) and 4(d) are consistent with the theoretical predictions.

When light incidents along the negative y axis ($\beta = 90^\circ$), Eqs. (14) and (15) are greatly simplified and become

$$\overline{S_3^R} = -2\pi \frac{\mathrm{Re}\left(\gamma^* \alpha_{ee}^{zz}\right)}{C_3}, \tag{18}$$

$$\overline{S_3^L} = 2\pi \frac{\mathrm{Re}\left(\gamma^* \alpha_{ee}\right)^{zz}}{C_3}, \tag{19}$$

$$C_3 = \frac{4}{3}\pi \mathrm{Re}\left[\gamma^* \gamma + \alpha_{ee}^{zz*}\alpha_{ee}^{zz} + \alpha_{mm}^{xx*}\alpha_{mm}^{xx}\right]. \tag{20}$$

It indicates that the bianisotropy (represented by γ) of the particle determines the polarization states of the scattered far field at $\beta = 90^\circ$. The polarization state is affected by the components of the polarizability tensors that is the inherent characteristic of the particle related to the size of the particle and the frequency of the incident light. Figure 5(a) shows the dependence of $\overline{S_3}$ on the height h of the bianisotropic particle. The frequency of the incident polarized light is 2.55 GHz. The diameter and height of the ceramic disk are $R = 15$ and $H = 12$ mm. The diameter of the hollow is $r = 9.4$ mm. The red and blue curves correspond to the left and right hemispheres, respectively. It is clear that $\overline{S_3}$ of the left and right hemispheres are opposite. There is a good agreement between theoretical and simulation results. The difference is mainly induced by neglecting the higher-order moments of the bianisotropic particle. $\overline{S_3}$ reaches the maximum at $h = 4.5$ mm. Similar to the above analysis, we investigate the change in $\overline{S_3}$ with the frequency f from 2.25 to 2.85 GHz as shown in Fig. 5(b). The diameter and height of the ceramic disk are $R = 15$ and $H = 12$ mm. The diameter and height of the hollow are $r = 9.4$ and $h = 4.5$ mm. The effect of perfect transverse spin splitting is obvious at $f = 2.55$ GHz which is off the resonant frequency of the particle as illustrated in Figs. 3(a) and 3(b). The perfect

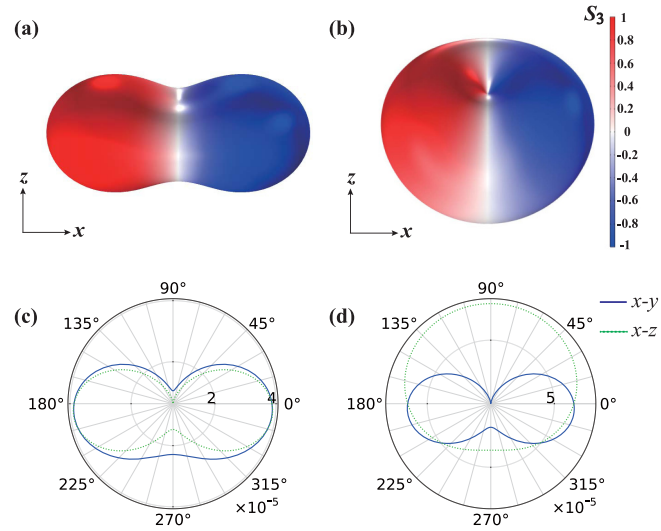

FIG. 6. Scattered electric field intensity and normalized Stokes polarization parameter S_3 distribution of perfect transverse spin splitting by transverse spin (a) electric and (b) magnetic dipole moments. Two-dimensional scattering diagram of the bianisotropic particle on the x-y plane and the x-z plane for the transverse spin (c) electric and (d) magnetic dipole moments.

transverse spin splitting at $f = 2.55$ GHz accords closely with our prediction that is achieved by the combination of different dipoles.

There are two methods to achieve the circular polarization separation in the x direction by constructing the transverse spin electric and magnetic dipole moments, respectively. Figure 6(a) shows the scattered electric field intensity and the normalized Stokes polarization parameter S_3 distributions of the perfect transverse spin splitting. The distance from the origin of coordinates corresponds to the scattered electric field intensity and the color represents the Stokes parameter S_3. The bianisotropic particle consists of a ceramic disk and a hollow with $R = 15$, $H = 12$, $r = 9.4$, and $h = 4.5$ mm. The frequency of the incident polarized light is 2.55 GHz. There is obvious opposite polarization in the opposite hemisphere that results from the transverse spin electric dipole moment. The pure linear polarizations are located on the planes with $\varphi = \pm 90^\circ$, which split the polarization of scattered far field into two hemispheres with opposite handedness. In addition to the transverse spin electric dipole moment, the transverse spin magnetic dipole moment $\mathbf{m} = (m_x, m_y, m_z)^T = (0, \pm i, 1)^T$ could be constructed approximatively when the incident electric field is the x polarized [$A = 1$, $B = 0$, and $\beta = 90^\circ$ in Eqs. (1) and (2)]. The size of the bianisotropic particle remains unchanged. The frequency of the incident polarized light is 2.5 GHz. The transverse spin splitting is directly observed in Fig. 6(b). It indicates that constructing the transverse spin magnetic dipole moment is also an effective method to realize the transverse spin splitting. The results are consistent with the previous theoretical analysis. Figures 6(c) and 6(d) depict the two-dimensional scattering diagram on the x-y plane and the x-z plane for the perfect transverse spin splitting induced by the transverse spin electric and magnetic dipole moments, respectively. Furthermore, the perfect transverse

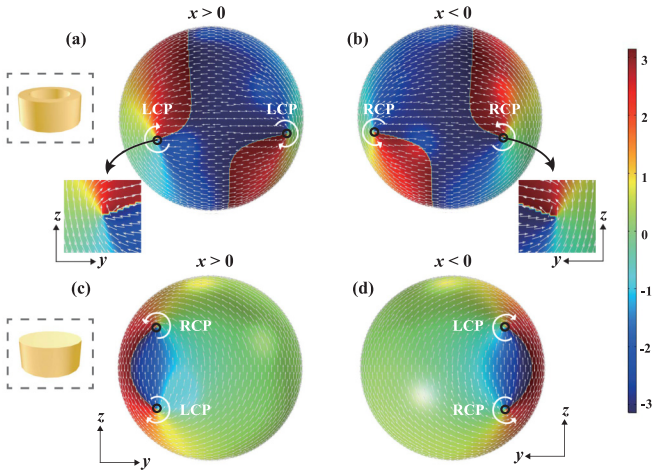

FIG. 7. (a) and (b) C points in the right ($x > 0$) and left ($x < 0$) hemispheres of the scattered far field by the bianisotropic particle, respectively. (c) and (d) C points in the right ($x > 0$) and left ($x < 0$) hemispheres of scattered far field by the ceramic disk, respectively.

spin splitting is accompanied by the transversely symmetrical intensity distribution in the x direction.

V. POLARIZATION SINGULARITIES

To further understand the polarization properties, we investigate the polarization singularities in the scattering field of the bianisotropic particle and the ceramic disk. The bianisotropic particle consists of a ceramic disk and a hollow with $R = 15$, $H = 12$, $r = 9.4$, and $h = 4.5$ mm. The diameter and height of the ceramic disk are $R = 15$ and $H = 12$ mm. The frequency of the incident polarized light is 2.55 GHz and the incident angle is $\beta = 90^\circ$. It is an effective way to describe a C point by the polarization ellipse and the phase of the scalar field $\Phi = \mathbf{E} \cdot \mathbf{E} = E^2 e^{i\phi}$. C points in the right hemisphere ($x > 0$) of the scattered far field by the bianisotropic particle are depicted in Fig. 7(a). The color represents the phase of $\mathbf{E} \cdot \mathbf{E}$. The two C points with the phase topological indices of -1 lie on the right hemisphere. Besides, the line segments denote the major axis of the polarization ellipse. The two C points are of the lemon type with the polarization topological index of $+1/2$. The results agree well with our theoretical prediction as shown in Fig. 2(g). The interference of the induced dipole modes results in the emergence of C points in the scattered far-field. Figure 7(b) shows C points in the left hemisphere ($x < 0$) with the phase topological indices of $+1$ and the polarization topological index of $+1/2$, respectively. The phase topological indices in the opposite hemisphere are opposite due to the perfect transverse spin splitting. Figures 7(c) and 7(d) depict C points in the right and left hemispheres of the scattered far field of the simple ceramic disk. The two C points have phase topological indices of -1 and $+1$ in both the right and the left hemispheres. The polarization topological indices of C points are all $+1/2$. It can be seen from Eqs. (18) and (19) that the spin state of the scattered far field of the disk is not split at $\beta = 90^\circ$ due to the absence of bianisotropy ($\gamma = 0$). The perfect transverse spin splitting is referred to as one kind of giant spin Hall effect of light with the obvious shift of the polarization singularities. It suggests that C points with the same phase topological index are located on the same hemisphere when the perfect transverse spin splitting occurs.

VI. CONCLUSION

To summarize, we demonstrate that a perfect transverse spin splitting effect could be realized by a bianisotropic particle. The two types of transverse spin dipole moments can be constructed to realize the perfect transverse spin splitting, which relies on the longitudinal dipole moments induced by the strong magnetoelectric coupling. Based on the dipole model, we have given a general description of the average polarization state of the scattered far field and presented the spin Hall effect of light. Besides, the perfect transverse spin splitting is highly related to the separation of polarization singularities, e.g., C points with the same phase topological index are located on the same hemisphere. The designed particle can be considered as a circular dipole emitter which could be used in chiral electromagnetic systems. Similar circular dipole sources have been exploited in spin-deterministic waveguide coupling [39,40], polarization-tailored optical switching [41], and chirality-induced optical isolators [42]. These applications are based on the so-called spin-momentum locking, that is, the spin of the circular dipole must match the intrinsic spin of the field in the device [43–45]. We believe that the proposed method to achieve the perfect transverse spin splitting through bianisotropic particles is promising for light manipulation, polarization sorters, optical sensing, and spin-based devices.

ACKNOWLEDGMENTS

This work was supported by the National Natural Science Foundation of China (Grants No. 11874132, No. 12074087, and No. U1931121), Natural Science Foundation of Heilongjiang Province in China (Grants No. LH2021A008 and No. ZD2020F002), 111 project to the Harbin Engineering University (Grant No. B13015), and Fundamental Research Funds for the Central Universities (Grants No. 3072021CFT2505 and No. 3072021CFT2501).

[1] O. G. Rodríguez-Herrera, D. Lara, K. Y. Bliokh, E. A. Ostrovskaya, and C. Dainty, Phys. Rev. Lett. **104**, 253601 (2010).

[2] S. Nechayev, P. Woźniak, M. Neugebauer, R. Barczyk, and P. Banzer, Laser Photonics Rev. **12**, 1800109 (2018).

[3] D. Vercruysse, Y. Sonnefraud, N. Verellen, F. B. Fuchs, G. D. Martino, L. Lagae, V. V. Moshchalkov, S. A. Maier, and P. V. Dorpe, Nano Lett. **13**, 3843 (2013).

[4] Z. Xi, L. Wei, A. J. L. Adam, H. P. Urbach, and L. Du, Phys. Rev. Lett. **117**, 113903 (2016).

[5] S. Nechayev, M. Neugebauer, M. Vorndran, G. Leuchs, and P. Banzer, Phys. Rev. Lett. **121**, 243903 (2018).

[6] A. Bag, M. Neugebauer, P. Woźniak, G. Leuchs, and P. Banzer, Phys. Rev. Lett. **121**, 193902 (2018).

[7] M. Neugebauer, P. Woźniak, A. Bag, G. Leuchs, and P. Banzer, Nat. Commun. **7**, 11286 (2016).

[8] M. Neugebauer, S. Nechayev, M. Vorndran, G. Leuchs, and P. Banzer, Nano Lett. **19**, 422 (2019).

[9] S. S. Kruk, M. Decker, I. Staude, S. Schlecht, M. Greppmair, D. N. Neshev, and Y. S. Kivshar, ACS Photonics **1**, 1218 (2014).

[10] K. Y. Bliokh, F. J. Rodríguez-Fortuo, F. Nori, and A. V. Zayats, Nat. Photonics **9**, 796 (2015).

[11] P. Shi, L. Du, C. Li, A. V. Zayats, and X. Yuan, Proc. Natl. Acad. Sci. USA **118**, e2018816118 (2021).

[12] K. Y. Bliokh, Y. Gorodetski, V. Kleiner, and E. Hasman, Phys. Rev. Lett. **101**, 030404 (2008).

[13] H. Onur and K. Paul, Science **319**, 787 (2008).

[14] X. Yin, Z. Ye, J. R. J, Y. Wang, and X. Zhang, Science **339**, 1405 (2013).

[15] X. Ling, X. Zhou, K. Huang, Y. Liu, C. W. Qiu, H. Luo, and S. Wen, Rep. Prog. Phys. **80**, 066401 (2017).

[16] S. Nechayev, J. S. Eismann, M. Neugebauer, and P. Banzer, ACS Photonics **7**, 581 (2020).

[17] D. O'connor, P. Ginzburg, F. J. Rodríguez-Fortuño, G. A. Wurtz, and A. V. Zayats, Nat. Commun. **5**, 5327 (2014).

[18] T. Feng, S. Yang, N. Lai, W. Chen, D. Pan, W. Zhang, A. A. Potapov, Z. Liang, and Y. Xu, Phys. Rev. B **102**, 205428 (2020).

[19] Y. Ra'di and S. A. Tretyakov, New J. Phys. **15**, 053008 (2013).

[20] R. Alaee, M. Albooyeh, A. Rahimzadegan, M. S. Mirmoosa, Y. S. Kivshar, and C. Rockstuhl, Phys. Rev. B **92**, 245130 (2015).

[21] R. Alaee, M. Albooyeh, M. Yazdi, N. Komjani, C. Simovski, F. Lederer, and C. Rockstuhl, Phys. Rev. B **91**, 115119 (2015).

[22] J. Vehmas, Y. Ra'di, A. O. Karilainen, and S. A. Tretyakov, IEEE T. Antenn. Propag. **61**, 3747 (2013).

[23] C. Pfeiffer and A. Grbic, Phys. Rev. Appl. **2**, 044011 (2014).

[24] L. Peng, L. Duan, K. Wang, F. Gao, L. Zhang, G. Wang, Y. Yang, H. Chen, and S. Zhang, Nat. Photonics **13**, 878 (2019).

[25] A. Epstein and G. V. Eleftheriades, in *2016 IEEE International Symposium on Antennas and Propagation (APSURSI), Fajardo, Puerto Rico, 2016* (IEEE, Piscataway, NJ, 2016), pp. 97–98.

[26] A. Epstein and G. V. Eleftheriades, IEEE T. Antenn. Propag. **64**, 3880 (2016).

[27] D. V. Zhirihin, S. V. Li, D. Y. Sokolov, A. P. Slobozhanyuk, M. A. Gorlach, and A. B. Khanikaev, Opt. Lett. **44**, 1694 (2019).

[28] W. Li, J. Liu, Y. Gao, K. Zhou, and S. Liu, Phys. Rev. A **102**, 063527 (2020).

[29] S. Tsesses, E. Ostrovsky, K. Cohen, B. Gjonaj, N. H. Lindner, and G. Bartal, Science **361**, 993 (2018).

[30] Y. Zhang, A. Chen, W. Liu, C. W. Hsu, B. Wang, F. Guan, X. Liu, L. Shi, L. Lu, and J. Zi, Phys. Rev. Lett. **120**, 186103 (2018).

[31] W. Liu, B. Wang, Y. Zhang, J. Wang, M. Zhao, F. Guan, X. Liu, L. Shi, and J. Zi, Phys. Rev. Lett. **123**, 116104 (2019).

[32] A. Chen, W. Liu, Y. Zhang, B. Wang, X. Liu, L. Shi, L. Lu, and J. Zi, Phys. Rev. B **99**, 180101(R) (2019).

[33] W. Ye, Y. Gao, and J. Liu, Phys. Rev. Lett. **124**, 153904 (2020).

[34] A. Garcia-Etxarri, ACS Photonics **4**, 1159 (2017).

[35] W. Chen, Y. Chen, and W. Liu, Laser Photonics Rev. **14**, 2000049 (2020).

[36] J. Peng, W. Liu, and S. Wang, Phys. Rev. A **103**, 023520 (2021).

[37] M. Dennis, Opt. Commun. **213**, 201 (2002).

[38] M. V. Berry, J. Opt. A: Pure Appl. Opt. **6**, 675 (2004).

[39] M. F. Picardi, A. Manjavacas, A. V. Zayats, and F. J. Rodríguez-Fortuño, Phys. Rev. B **95**, 245416 (2017).

[40] I. Söllner, S. Mahmoodian, S. L. Hansen, L. Midolo, A. Javadi, G. Kiršanskė, T. Pregnolato, H. El-Ella, E. H. Lee, J. D. Song *et al.*, Nat. Nanotechnol. **10**, 775 (2015).

[41] M. Neugebauer, T. Bauer, P. Banzer, and G. Leuchs, Nano Lett. **14**, 2546 (2014).

[42] C. Sayrin, C. Junge, R. Mitsch, B. Albrecht, D. O'Shea, P. Schneeweiss, J. Volz, and A. Rauschenbeutel, Phys. Rev. X **5**, 041036 (2015).

[43] M. F. Picardi, A. V. Zayats, and F. J. Rodríguez-Fortuño, Phys. Rev. Lett. **120**, 117402 (2018).

[44] M. Neugebauer, P. Banzer, and S. Nechayev, Sci. Adv. **5**, eaav7588 (2019).

[45] L. Marrucci, Nat. Phys. **11**, 9 (2015).